doi:10.1016/j.jmb.2011.01.017 J. Mol. Biol. (2011) 407, 138–148

Contents lists available at www.sciencedirect.com

Journal of Molecular Biology

journal homepage: http://ees.elsevier.com.jmb

Constraining Enzyme Conformational Change by an Antibody Leads to Hyperbolic Inhibition

David Oyen, Vasundara Srinivasan, Jan Steyaert and John N. Barlow*

Structural Biology Brussels, Vrije Universiteit Brussel, Pleinlaan 2, 1050 Brussels, Belgium
Department of Molecular and Cellular Interactions, Structural Biology Brussels, VIB, Pleinlaan 2, 1050 Brussels, Belgium

Received 15 June 2010;
received in revised form
21 December 2010;
accepted 7 January 2011
Available online
14 January 2011

Edited by A. G. Palmer III

Keywords:
allosteric effector;
dihydrofolate reductase;
transient kinetics;
crystal structure;
antibody

Although it has been known for many years that antibodies display properties characteristic of allosteric effectors, the molecular mechanisms responsible for these effects remain poorly understood. Here, we describe a single-domain antibody fragment (nanobody) that modulates protein function by constraining conformational change in the enzyme dihydrofolate reductase (DHFR). Nanobody 216 (Nb216) behaves as a potent allosteric inhibitor of DHFR, giving rise to mixed hyperbolic inhibition kinetics. The crystal structure of Nb216 in complex with DHFR reveals that the nanobody binds adjacent to the active site. Half of the epitope consists of residues from the flexible Met20 loop. This loop, which ordinarily oscillates between occluded and closed conformations during catalysis, assumes the occluded conformation in the Nb216-bound state. Using stopped flow, we show that Nb216 inhibits DHFR by stabilising the occluded Met20 loop conformation. Surprisingly, kinetic data indicate that the Met20 loop retains sufficient conformational flexibility in the Nb216-bound state to allow slow substrate turnover to occur.

© 2011 Elsevier Ltd. All rights reserved.

Introduction

Allosteric effectors are molecules that modulate the activities of enzymes and receptors by binding outside the active site.[1–3] Allosteric control of metabolic and signalling pathways is widespread in biology and disease, and there is much interest in the discovery of synthetic allosteric effectors for use in therapy.[4] It has been known for many years that antibodies can also behave as allosteric effectors, giving rise to kinetic effects such as activation or noncompetitive inhibition of enzymes and receptors.[5–8] Such properties have been widely exploited to experimentally manipulate and characterise allosteric systems[9] and could potentially be put to therapeutic use.[10] Autoantibodies (i.e., antibodies that recognise self rather than foreign proteins) can also behave as allosteric effectors and are implicated in immune diseases.[11,12] Despite this, the molecular mechanisms of allosteric control are not well understood.

Part of the difficulty in determining the molecular basis for allosteric effector antibodies have been the large size and complexity of the systems studied so far (e.g., Fab binding to G-protein coupled receptors). We therefore turned to a simpler system consisting of single-domain antibody fragments (nanobodies) raised against the dihydrofolate reductase (DHFR) from *Escherichia coli*. Nanobodies are derived from the variable (V_{HH}) domains of the heavy-chain antibodies of camelids.[13] Their small size (14 kDa)

**Corresponding author*. GSK Biologicals, Rue de l'institute 89, 1330 Rixensart, Belgium. E-mail address: john.n.barlow@gskbio.com.

Abbreviations used: DHFR, dihydrofolate reductase; Nb216, nanobody 216; DHF, 7,8-dihydrofolate; THF, 5,6,7,8,-tetrahydrofolate; CDR, complementarity-determining region; PDB, Protein Data Bank; FRET, Förster resonance energy transfer.

0022-2836/$ - see front matter © 2011 Elsevier Ltd. All rights reserved.

and high solubility greatly facilitate an analysis of their molecular properties (e.g., by NMR).

DHFR catalyses the reduction of 7,8-dihydrofolate (DHF) to 5,6,7,8,-tetrahydrofolate (THF) using reduced nicotinamide dinucleotide phosphate (NADPH) as cofactor (Fig. 1). The structural and dynamic changes undergone by DHFR during catalysis have been characterised extensively.[15–17] Similar to many enzymes, DHFR contains a flexible active-site loop (the Met20 loop) that switches between different conformational states (termed the occluded and closed states) during catalysis. Presumably, this flexibility permits the rapid binding and dissociation of active-site ligands and, at the same time, increases the binding energy available for transition-state stabilisation.[18] In fact, there is considerable evidence that functional conformational flexibility is not localised to the active site but extends throughout the whole DHFR structure.[19] DHFR therefore affords an opportunity to investigate the relationships between structure, dynamics, and allosteric effects caused by nanobody binding to a relatively small and well-characterised enzyme. In the following, we dissect the inhibition mechanism of nanobody 216 (Nb216), which behaves as an allosteric inhibitor of DHFR. We show that Nb216 mechanically constrains conformational change in DHFR, leading to allosteric inhibition of cofactor binding.

Results

Hyperbolic inhibition of DHFR steady-state activity by Nb216

Nb216 was identified as a DHFR inhibitor during the screening of a collection of nanobodies derived from two immunised llamas. Nb216 shows nanomolar binding to apo-DHFR (Table 1). A detailed examination of the inhibitory properties of Nb216 shows that it gives rise to hyperbolic mixed inhibition kinetics (i.e., partial inhibition) with respect to NADPH (Fig. 2). Hyperbolic inhibition is characteristic of allosteric inhibitors (i.e., inhibitors that bind outside the active site[20,21]), although nonallosteric mechanisms can also be invoked in other enzymes (e.g., half-of-the-sites binding to dimeric enzymes[7]). The extent of inhibition at infinite Nb216 concentration was estimated by fitting the inhibition data to Eq. (1):[7]

$$y = a\frac{(1 + [\mathrm{Nb}] / K_{\mathrm{num}})}{(1 + [\mathrm{Nb}] / K_{\mathrm{denom}})} \quad (1)$$

where $y = 1/k_{cat}$ or K_m/k_{cat} (depending on the plot), Nb = Nb216 concentration, and K_{num} and K_{denom} are fitted parameters (Table 2). The ratio K_{denom}/K_{num} gives the relative change in apparent $(k_{cat}/K_m)^{NADPH}$ or apparent $(k_{cat})^{NADPH}$ upon binding of Nb216. Nb216 is a potent inhibitor, and Nb216 binding reduces $(k_{cat}/K_m)^{NADPH}$ and $(k_{cat})^{NADPH}$ ~100-fold and ~50-fold, respectively, upon saturation. It should be noted that a mechanistic interpretation of K_{num} and K_{denom} is nontrivial for enzymes that show complex kinetic mechanism, such as DHFR.[7] We therefore turned to pre-steady-state approaches to further examine the mechanism of Nb216 (see the text below).

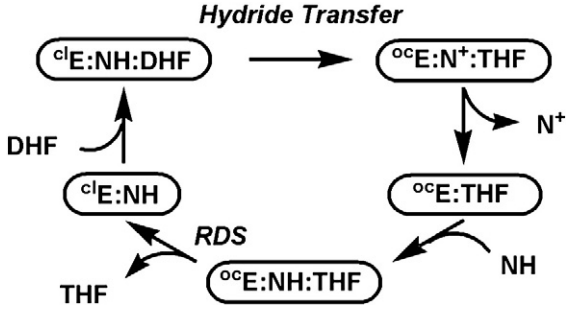

Fig. 1. Catalytic intermediates of *E. coli* DHFR during steady-state turnover under saturating substrate and cofactor conditions.[14] Note that the rate-determining step corresponds to product (THF) release. NH and N^+ refer to the reduced and oxidised cofactors NADPH and $NADP^+$, respectively. Also indicated are the closed (^{cl}E) and occluded (^{oc}E) Met20 loop conformational states. This figure was adapted from Fierke *et al.*[14]

Table 1. Data on Nb216 binding to apo-DHFR (as determined by surface plasmon resonance at 25 °C)

	k_{on} (μM^{-1} s^{-1})	k_{off} (s^{-1})	K_d (nM)
Nb216	0.086 ± 0.011[a]	0.003 ± 0.001	34 ± 17

[a] Standard error ($n = 2$).

Nb216 epitope undergoes conformational change during catalysis

We identified the Nb216 epitope by solving the crystal structure of the E:Nb216 complex. Nb216 binds on the DHFR surface to a planar epitope adjacent to the substrate and cofactor binding pockets (Fig. 3). The Nb216 paratope contains residues from all three complementarity-determining region (CDR) loops and framework 2. Half of the epitope consists of residues from the Met20 loop (based on buried surface area[22]). The Met20 loop is located at the centre of the epitope and makes numerous hydrogen bonds and hydrophobic interactions with the nanobody (Fig. 4 and Table 3). The remainder of the epitope is made up of residues from the GH and FG loops, which flank either side of the Met20 loop. A comparison of the E:Nb216 binary complex crystal structure and the E:$NADP^+$:

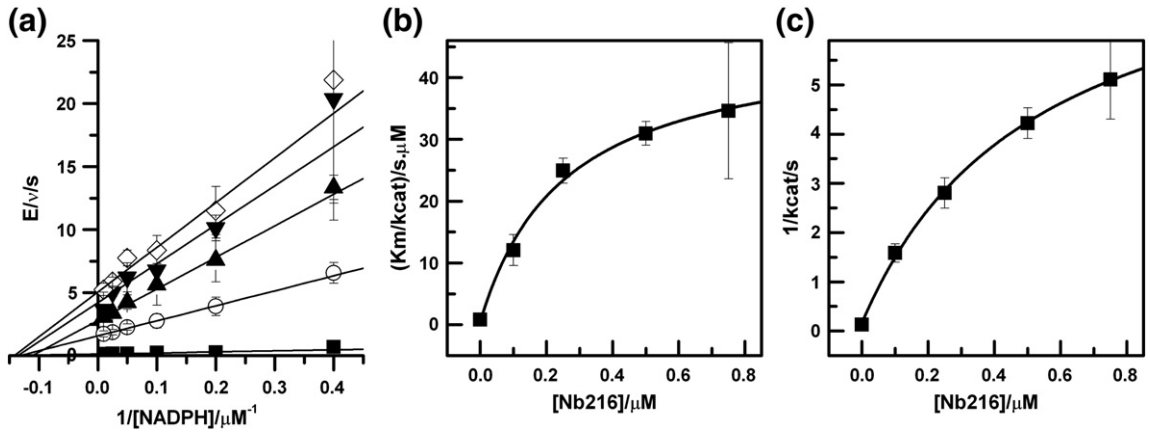

Fig. 2. Steady-state inhibition kinetics of Nb216. (a) Double-reciprocal plot of initial steady-state velocity *versus* NADPH concentration at 0 μM (■), 0.1 μM (○), 0.25 μM (▲), 0.5 μM (▼), and 0.75 μM (◊) Nb216. (b and c) Plots of $(K_m/k_{cat})^{NADPH}$ and $(1/k_{cat})^{NADPH}$ *versus* [Nb216] at 10 μM H_2F (pH 7.0) at 25 °C . Nonlinear fits to Eq. (1) are shown. Error bars represent the standard deviation from two experiments performed on the same day.

folate ternary complex crystal structure [Protein Data Bank (PDB) code 1RX2] shows that none of the DHFR chemical groups directly interacting with Nb216 also interacts directly with $NADP^+$ or folate (Table 3). Three DHFR residues (A19, M20, and W22) do make binding interactions with both $NADP^+$ (in the E:$NADP^+$:folate structure) and Nb216 (in the DHFR:Nb216 structure) (Fig. 5 and Table 3). However, these three residues interact with $NADP^+$ and Nb216 through different chemical groups (Fig. 5). A19 hydrogen bonds to $NADP^+$ via its main-chain amide group, while it bonds to Nb216 via its main-chain carbonyl group. M20 and W22 both make hydrophobic interactions with $NADP^+$ via their side chains, whereas these residues hydrogen bond to Nb216 via their main-chain carbonyls.

A comparison of the α-carbon trace for DHFR in the E:Nb216 structure with other DHFR crystal structures shows that the Met20 loop is in an occluded state in complex with the antibody (Figs. 6 and 7a). The Met20 loop shows strong electron density in the E:Nb216 structure (Fig. 7b), in marked contrast to the disordered Met20 loop in the apo-DHFR crystal, giving rise to weak electron density.[16] Hydrogen bonds that stabilise the occluded conformation in other occluded state crystal structures are also present in the E:Nb216 structure (Fig. 7c). No substantial distortion is seen in either the substrate binding pocket or the adenosine binding pocket (Fig. 6). Marginal deviations in the main-chain conformation at the CD and FG loops are observed in the E:Nb216 structure (Fig. 6). These deviations are likely crystal packing artefacts because both the CD loop and the FG loop are involved in crystal packing contacts. The conformations of these loops are known to be strongly influenced by packing effects on other DHFR crystal structures.[16]

Taken together, all structural data indicate that Nb216 binds to and stabilises the occluded DHFR state without a significant distortion of DHFR structure. Binding of the nicotinamide moiety of NADPH to the active site is sterically blocked by the Met20 loop when it assumes the occluded conformation.[16] Therefore, we postulate that Nb216

Table 2. Steady-state inhibition kinetic parameters from Eq. (1)

	K_m/k_{cat} plot	$1/k_{cat}$ plot
a (μM s^a or s^b)	0.47 ± 1.53[c]	0.163 ± 0.074
K_{num} (μM)	0.0026 ± 0.0087	0.0100 ± 0.0051
K_{denom} (μM)	0.255 ± 0.067	0.528 ± 0.063

[a] Units for the K_m/k_{cat} plot.
[b] Units for the $1/k_{cat}$ plot.
[c] Standard error from nonlinear curve fitting.

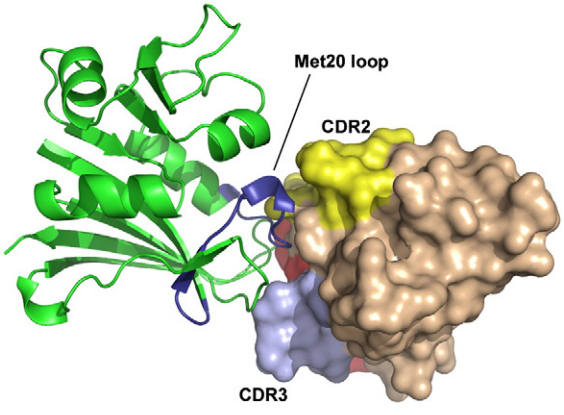

Fig. 3. Crystal structure of the DHFR:Nb216 binary complex. Nb216 is shown in surface representation; residues in CDR2 and CDR3 are shown in yellow and blue, respectively. The Met20 loop of DHFR (ribbon representation) is highlighted in dark blue.

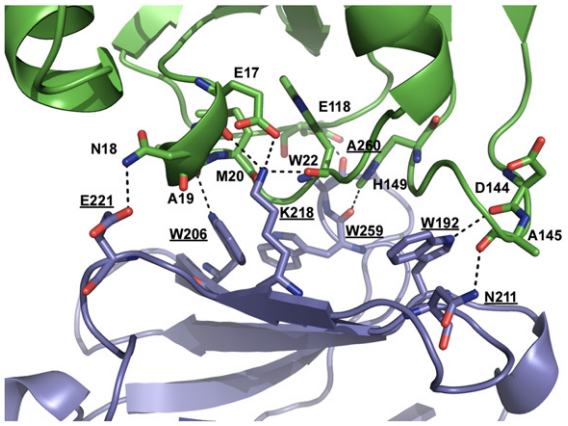

Fig. 4. Detailed view of the binding interface between DHFR (green) and Nb216 (blue). Residues participating in polar interactions are indicated (Nb216 residues are underlined).

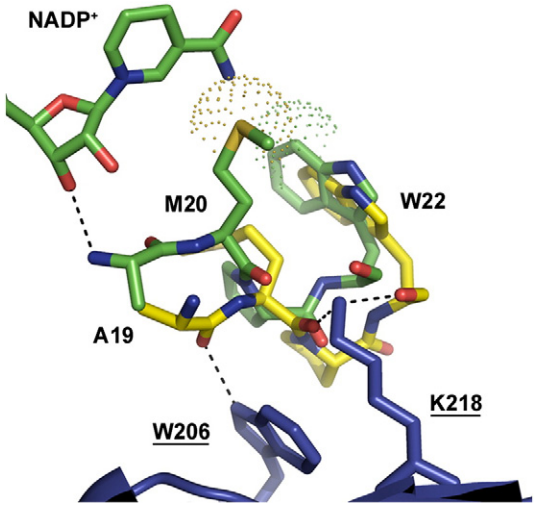

Fig. 5. Detailed view of the DHFR:Nb216 binary complex (yellow and blue, respectively) and the DHFR:NADP$^+$:folate ternary complex (green; PDB code 1RX2; folate not shown) in superposition. The principal binding interactions of Ala19, Met20, and Trp22 with Nb216 and NADP$^+$ are shown (hydrogen bonds, broken lines; principal hydrophobic contact atoms, dotted spheres).

inhibits DHFR catalysis by inhibiting the formation of the closed ^{cl}E:NADPH and ^{cl}E:NADPH:DHF intermediates (Fig. 1).

Nb216 blocks nicotinamide binding in the E:NADPH holoenzyme

We confirmed that Nb216 inhibits the formation of the closed Met20 loop conformation by examining the binding kinetics of NADPH. Binding of NADPH to DHFR to form the closed E:NADPH complex gives rise to a Förster resonance energy transfer (FRET) signal that can be followed by stopped-flow fluorescence at $\lambda > 400$ nm[14] (Fig. 8a, curve I). The FRET signal originates from interactions between DHFR tryptophan residues and the bound nicotinamide

Table 3. DHFR:Nb216 interactions

DHFR residue	Secondary structure	Nb216 residue	Framework or CDR loop	Type of interaction	Distance (Å)	Buried surface area (Å^2)[a]
E17 OE2	Met20 loop	K218 NZ	CDR2	H-bond	2.8	9
E17 O	Met20 loop	K218 NZ	CDR2	H-bond	2.9	
N18 ND2	Met20 loop	E221 OE2	CDR2	H-bond	2.8	18
A19 O[b]	Met20 loop	W206 NE1	Framework 2	H-bond	2.9	18
M20 O[c]	Met20 loop	K218 NZ	CDR2	H-bond	2.6	12
P21	Met20 loop	W206	Framework 2	Hydrophobic	3.8	90
P21	Met20 loop	M209	Framework 2	Hydrophobic	3.6	
W22 O[d]	Met20 loop	K218 NZ	CDR2	H-bond	2.7	12
W22	Met20 loop	M209	Framework 2	Hydrophobic	4.0	
N23	Met20 loop	W192	CDR1	Hydrophobic	3.8	65
N23	Met20 loop	M209	Framework 2	Hydrophobic	4.1	
E118 N	FG loop	A260 O	CDR3	H-bond	2.7	52
D144 O	GH loop	W192 NE1	CDR1	H-bond	3.0	10
A145 O	GH loop	N211 ND2	CDR2	H-bond	2.8	57
Q146	GH loop	W192	CDR1	Hydrophobic	3.5	46
S148	GH loop	W192	CDR1	Hydrophobic	3.8	46
S148	GH loop	M209	Framework 2	Hydrophobic	3.6	
H149 NE2	GH loop	W259 O	CDR3	H-bond	3.1	46

[a] Buried surface area was determined by ProtorP.[22]
[b] A19 hydrogen bonds to the ribosyl O3′ group of NADP$^+$ in the E:NADP$^+$:folate crystal structure (PDB code 1RX2) with its main-chain amide group.
[c] M20 interacts with folate and NADP in the E:NADP$^+$:folate crystal structure (PDB code 1RX2) via hydrophobic interactions with its side chain.
[d] W22 interacts with folate in the E:NADP$^+$:folate crystal structure (PDB code 1RX2) via hydrophobic interactions involving its side chain. In E:Nb216, the side chain does not interact with Nb216.

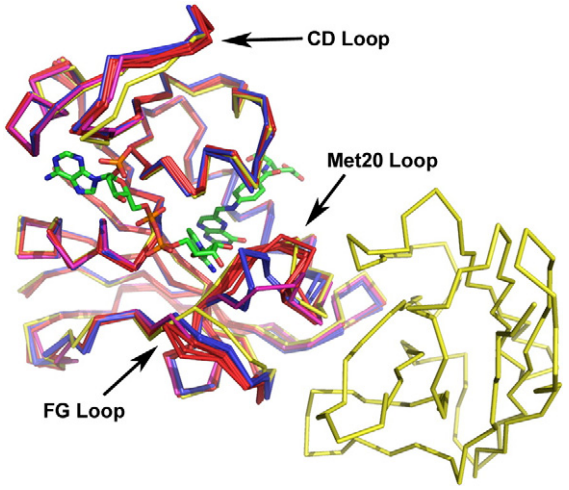

Fig. 6. α-Carbon traces of the DHFR:Nb216 crystal structure (yellow) aligned to a selection of Nb216-free DHFR crystal structures: occluded conformations (red; PDB codes 1RX4, 1RX5, 1RX6, 1RX7, 1RF7, and 1JOM), closed conformations (blue; PDB codes 1RX1, 1RX2, and 1RX3), and open conformation (pink; PDB code 1RA3). $NADP^+$ and folate are shown in stick representation for reference.

moiety of NADPH. The amplitude of the FRET transient is greatly attenuated in the reaction of NADPH with the E:Nb216 complex (Fig. 8a, curve II). Therefore, Nb216 inhibits nicotinamide binding. However, Nb216 does not inhibit the binding of the adenosine moiety of NADPH. This is apparent from an examination of the stopped-flow progress curves with detection of tryptophan fluorescence emission at $\lambda > 305$ nm (Fig. 8a, curves III and IV). At these wavelengths, NADPH binding transients are observed upon mixing E:Nb216 with NADPH (Fig. 8a, curve IV). The amplitude of this NADPH binding transient is larger than that observed upon mixing E with NADPH (Fig. 8a, curve III). Presumably, the difference in amplitudes arises because FRET only makes a contribution to the detected signal when Nb216 is absent. Nb216 does not alter k_{obs} (Supplementary Fig. 1c). Therefore, Nb216 disrupts the binding of the nicotinamide moiety of NADPH (with loss of FRET), but not the binding of the adenosine moiety (which causes quenching of tryptophan fluorescence), consistent with stabilisation of the occluded Met20 loop conformation.

The rate of nicotinamide binding determines k_{cat} in the presence of Nb216

Having established that Nb216 disrupts the binding of the nicotinamide moiety of NADPH to DHFR, we next show that the binding of the nicotinamide moiety of NADPH determines k_{cat} in the presence of Nb216. The rates of the first two steps of the catalytic pathway (DHF binding

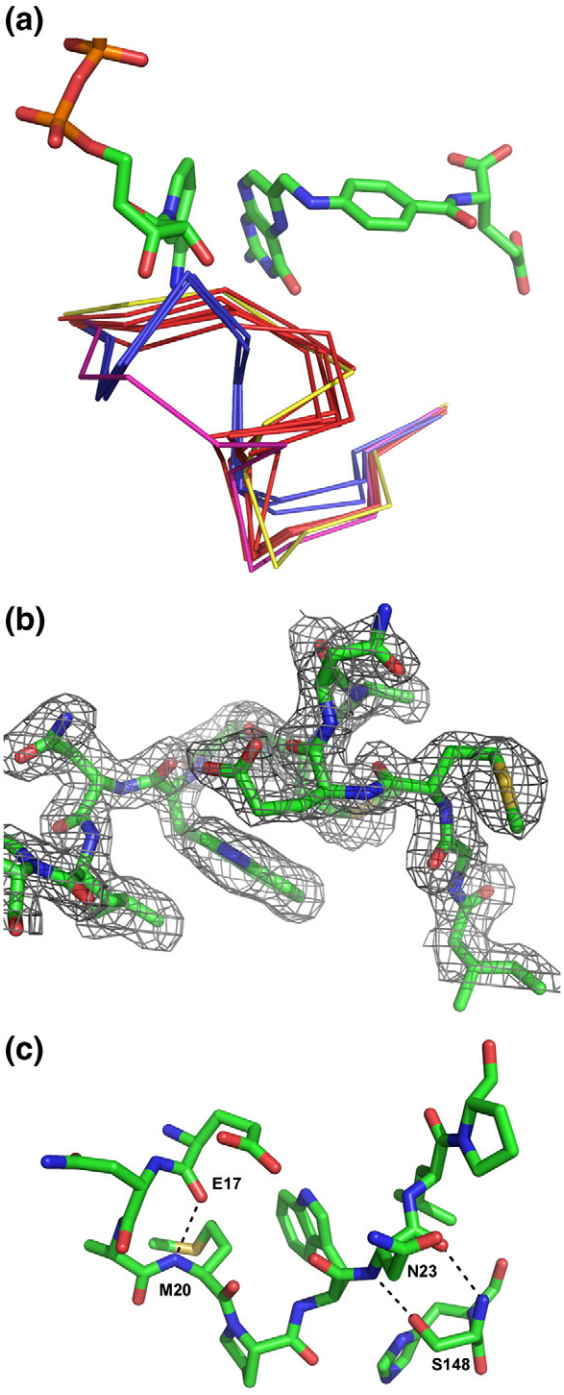

Fig. 7. (a) Highlight of Fig. 6, as viewed from above, showing the α-carbon traces of the Met20 loops. (b) Electron density map of the Met20 loop region in the E:Nb216 crystal structures, contoured at 1.0σ. (c) Met20 loop region in the E:Nb216 crystal structure, showing the characteristic hydrogen-bond pattern of the occluded conformation.

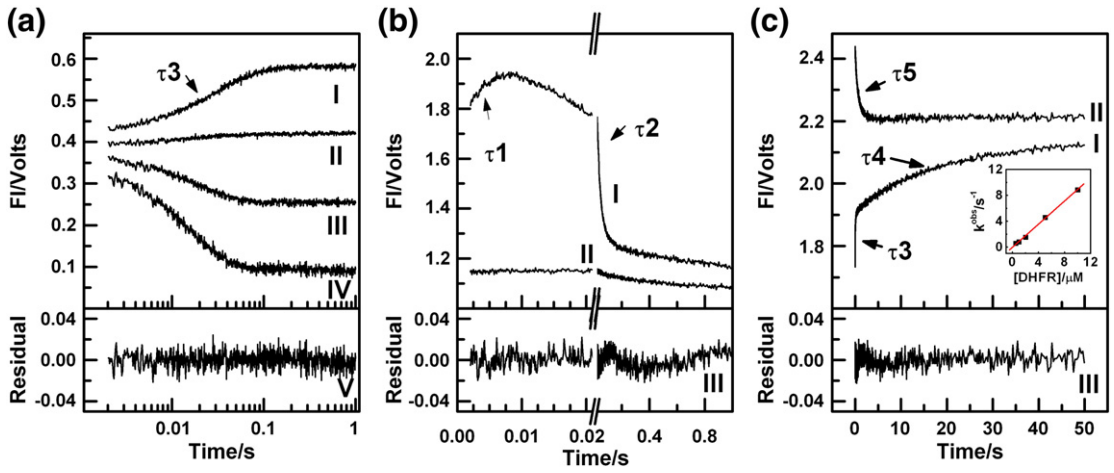

Fig. 8. Effect of Nb216 on DHFR transient kinetics. (a) Stopped-flow progress curves for NADPH binding to E (curves I and III) and E:Nb216 (curves II and IV), followed by FRET (curves I and II) or total emitted fluorescence (305-nm cutoff; curves III and IV). An offset was added to the progress curves for display purposes, but the same PMT voltage was used for each progress curve. Note that the amplitude of curve IV is larger than that of curve III due to loss of FRET. Curve V is a plot of residuals for fitting Eq. (3) ($n=1$) to the curve IV data. [DHFR] = 0.5 μM, [NADPH] = 5 μM, [Nb216] = 1 μM, 5 °C. (b) Stopped-flow FRET progress curves for the reaction of DHF with E:NADPH (curve I) and E:NADPH:Nb216 (curve II). Progress curves represent the mean of 14 shots. [DHFR] = 1 μM, [NADPH] = 20 μM, [DHF] = 4 μM, [Nb216] = 2 μM, 5 °C. Binding τ_1 and hydride transfer τ_2 transients are indicated. An offset was applied to curve II. Curve III is a plot of residuals for fitting Eq. (3) ($n=2$) to the curve I data. (c) Stopped-flow progress curves showing binding of NADPH to E (curve I) and binding of Nb216 to E:NADPH (curve II). [DHFR] = 2 μM, [NADPH] = 40 μM (curve I) and 100 μM (curve II), [Nb216] = 0.5 μM, 25 °C. Inset: Plot of k_{obs} *versus* [DHFR] for the τ_5 transient. Curve III is a plot of residuals for fitting Eq. (3) ($n=1$) to the curve II data.

to E:NADPH and subsequent hydride transfer; Fig. 1) can be measured by stopped flow at 278 K. At this temperature, DHF binding to E:NADPH gives rise to a monophasic fluorescence transient (τ_1; Fig. 8b, curve I). The τ_1 transient is succeeded by a slower FRET decay transient (τ_2) that results from the conversion of NADPH into $NADP^+$ during the hydride transfer step. It should be noted that the slowest step on the catalytic cycle under saturating concentrations of substrate and cofactor is the release of the product THF (Fig. 1). Neither transient was observed during the reaction of DHF with the preformed E:NADPH:Nb216 complex (Fig. 8b, curve II). The loss of the τ_1 DHF binding transient is unlikely to be caused by inhibition of DHF binding because Nb216 had little effect on the binding kinetics of DHF with E (Supplementary Fig. 1a and b). Similarly, hydride transfer is unlikely to rate determine the steady-state rate because no kinetic isotope effect was observed with [4′(*R*)-^{2}H] NADPH on either k_{cat} or k_{cat}/K_m in the presence of Nb216 (Supplementary Fig. 2). Instead, the loss of both τ_1 and τ_2 transients is readily explained by the slow rate-determining binding of the nicotinamide moiety of NADPH. It should be noted that both progress curves in Fig. 8b contain a slow transient (that follows τ_2 in curve I) of unknown origin.

Evidence for Met20 loop mobility in the E:NADPH:Nb216 complex

The hyperbolic inhibition of DHFR steady-state activity by Nb216 indicates that turnover can occur when Nb216 is bound to DHFR. Presumably, the nicotinamide moiety of NADPH must bind productively within the E:NADPH:DHF:Nb216 complex at a rate similar to k_{cat} ($\sim 0.1\ s^{-1}$). This is not possible unless the Met20 loop undergoes a conformational change from the occluded state to a nicotinamide-binding-competent state. We show here that the closed → occluded conformational change can take place in the Nb216-bound state. For this, we followed the reaction of E:NADPH holoenzyme (closed state) with Nb216 by stopped flow. During this reaction, we observe a FRET decay transient τ_5 (Fig. 8c, curve II). The FRET decay is consistent with the dissociation of the nicotinamide moiety from the DHFR active site. Indeed, the amplitude of the τ_5 transient is similar in magnitude (but of opposite sign) to the τ_3 FRET transient observed when NADPH binds to apo-DHFR to form the closed E:NADPH holoenzyme (Fig. 8c, curve I). Furthermore, the observed rate constant of the τ_5 transient is linearly dependent on the concentration of the E:NADPH complex (Fig. 8c, inset), indicating that we are observing a bimolecular association process

($k_{on}^{app} = 0.89 \pm 0.02\ \mu M^{-1}\ s^{-1}$; $k_{off}^{app} = 0.0 \pm 0.1\ s^{-1}$). The most plausible explanation for these data is that the closed → occluded conformation change takes place in the Nb216-bound state (Eq. (2)) at a rate at least as fast as k_{obs} (i.e., $k_3 > 10\ s^{-1}$):

$$^{c1}\text{E: NH} + \text{Nb} \underset{k_2}{\overset{k_1}{\rightleftharpoons}} {}^{c1}\text{E: NH : Nb} \underset{k4}{\overset{k_3}{\rightleftharpoons}} {}^{oc}\text{E: NH : Nb} \quad (2)$$

Other less plausible models are described in Supplementary Information. Taking the rate of formation of the closed E:NADPH:Nb216 complex to be similar to k_{cat} ($k_4 \sim 0.1\ s^{-1}$), we see that the occluded conformation is at least (10/0.1) 100-fold more stable than the closed conformation in the Nb216-bound state.

Discussion

We have shown here that hyperbolic inhibition by a single-domain antibody fragment is a direct consequence of constraining enzyme conformational change. Nb216 binds to the Met20 loop of DHFR, stabilising it in the occluded conformation (Figs. 6 and 7). The occluded Met20 loop sterically prevents the binding of the nicotinamide moiety of NADPH (Fig. 8a, curves I and II), leading to inhibition of turnover. No significant distortion of the substrate binding pocket or the adenosine binding pocket is apparent in the E:Nb216 crystal structure. Our stopped-flow data show that the binding kinetics of H_2F and the adenosyl moiety of NADPH are similar for both E and E:Nb216 complex (Fig. 8a; Supplementary Fig. 1). Therefore, Nb216 appears to stabilise an on-pathway conformation (DHFR conformation) rather than a novel off-pathway conformation.

The observed hyperbolic inhibition (Fig. 2) indicates that turnover takes place, albeit at a reduced rate, under saturating Nb216 concentrations (i.e., when Nb216 is bound to DHFR). But how can turnover occur in the Nb216-bound state if Nb216 blocks the binding of the nicotinamide moiety of NADPH? The simplest explanation is that the Met20 loop is still able to transiently assume a conformation that is competent to bind nicotinamide in the Nb216-bound state. The failure to detect the buildup of a nicotinamide-bound state in the presence of Nb216 by stopped flow (Fig. 8a, curve II; Fig. 8b, curve II), together with the large decrease in steady-state parameters under saturating Nb216, indicates that the nicotinamide-bound state is unstable under equilibrium or steady-state conditions. Similarly, the stopped-flow data of Fig. 8c indicate that the closed ^{cl}E:NADPH:Nb216 ternary complex is formed transiently upon mixing ^{cl}E:NADPH with Nb216.

Some ideas on the extent of structural change that would be necessary for the nicotinamide moiety to bind in the presence of Nb216 can be obtained from comparing the E:Nb216 and E:$NADP^+$:DHF crystal structures (the latter structure is a resemble model for the Michaelis complex) (Figs. 4 and 9). This comparison shows that a large proportion of the Nb216 epitope has a similar conformation in both structures. Binding of the nicotinamide moiety would require the loss of Nb216 binding interactions in the vicinity of the Met20 loop (e.g., those involving N18 and A19 of DHFR). Future studies should reveal exactly which bonding interactions are important for the stabilisation of the occluded loop and whether Nb216 can be mimicked by small-molecule allosteric inhibitors. It should be noted that the intracellular reducing environment of DHFR in eukaryotes and prokaryotes poses a considerable challenge for the development of therapeutic nanobodies.

Does Nb216 qualify as an allosteric effector? In order to do so, Nb216 should fulfill the following requirements:[1] (i) it should have a structure different from those of the substrate and the cofactor; (ii) it should elicit a change in a functional property of DHFR (viz. hyperbolic inhibition of catalysis); and (iii) it should bind at a site that is topographically distinct from the active site. Nb216 clearly fulfills the first and second requirements. The third requirement is less clear-cut because three DHFR residues (A19, M20, and W22) make binding interactions with both $NADP^+$ (in the E:$NADP^+$:folate structure) and Nb216 (in the DHFR:Nb216 structure) (Fig. 5 and Table 3). In our opinion, the fact that these three residues interact with $NADP^+$ and Nb216 through different chemical groups means that the binding

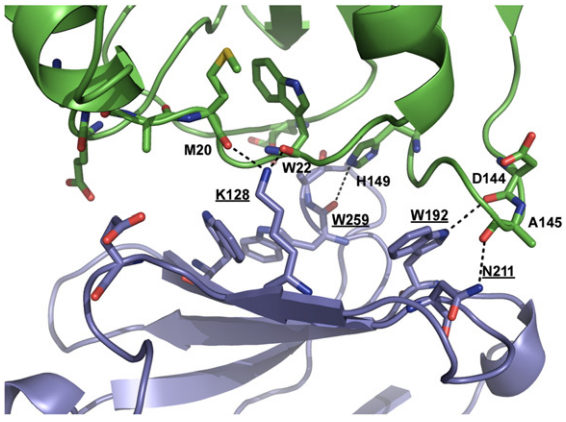

Fig. 9. Hypothetical model of Nb216 bound to DHFR in the closed Met20 loop conformation, illustrating likely loss of polar contact. The model was made by aligning the E:$NADP^+$:folate crystal structure (PDB code 1RX2) to the E:Nb216 crystal structure.

surfaces are topographically different. Therefore, Nb216 does qualify as an allosteric effector.

In Fig. 10, we show a simple catalytic pathway for DHFR in the presence of saturating concentrations of substrate and Nb216 that is consistent with all the data presented here. According to this mechanism, Nb216 remains bound to DHFR throughout the cycle. The rate-determining step corresponds to the conversion of the occluded Met20 loop conformation into the closed conformation within the Michaelis complex (E:NADPH:DHF:Nb216). The rate of this process is reduced by at least 3 orders of magnitude, from $\sim$2000 s^{-1} in the absence of Nb216[23] to $\sim$0.1 s^{-1} (i.e., k_{cat}) in the Nb216-bound state. Steady-state inhibition by Nb216 is mixed (both k_{cat}/K_m and k_{cat} are affected) because this step occurs before chemistry. It should be noted that kinetic models that describe the steady state under nonsaturating concentrations of substrate and Nb216 (e.g., k_{cat}/K_m conditions) are likely to be extremely complex, given the complex nature of the DHFR reaction in the absence of Nb216.[14]

It is both pragmatic and instructive to classify allosteric effector antibodies according to their epitope structures. Antibodies such as Nb216 (which we classify as a group 1 member) recognise epitopes that undergo substantial conformational change during catalysis. Such antibodies are likely to preferentially stabilise a particular enzyme conformation, thus altering the rates of particular steps on the catalytic pathway. Group 2 antibodies recognise epitopes that do not apparently undergo conformational change during the catalytic cycle. Antibodies that bind to such 'constant ground-state structure' epitopes could, nevertheless, influence catalysis by perturbing protein dynamics (i.e., by altering the conformational ensemble[24,25]), for example by sterically hindering particular conformers. Evidence indicating that antibodies can give rise to long-range dynamic effects comes from hydrogen-exchange experiments.[26] These show that antibodies can alter the rate of hydrogen exchange at regions distal to the epitope without any discernible change in antigen crystal structure. Group 3 antibodies recognise epitopes that have non-native-state conformations (i.e., they are distorted). The extent of the structural perturbation of antigen structure by antibodies is generally small and restricted to the epitope region.[27] Large distortions of structure are rare, presumably because it is thermodynamically costly to distort antigen structure from the ground state.[28] Long-range distortions in T7 DNA polymerase structure were observed upon binding to an inhibitory Fab.[29] In this case, inhibition was caused by Fab binding to residues that interact with DNA and by blocking of DNA binding, rather than via an allosteric effect. Distortion of antigen structure has also been implicated in the mechanism of a neutralising antibody against poliovirus.[30] Recently, an allosteric effector Fab antibody (Ab40) that partially inhibits the HGFA protease by stabilising an active-site loop (the 99 loop) in a conformation that impairs catalysis has been described.[31] The extent of inhibition (4-fold drop in K_m) is much smaller than that observed with Nb216, presumably because the altered 99 loop conformation represents a much smaller kinetic barrier than the trapped occluded Met20 loop. In passing, we note that small-molecule allosteric effectors are also known to stabilise distorted enzyme conformations.[32] These groupings of allosteric effector antibodies are both useful (because the epitope structure is well defined and relatively straightforward to determine), and they also highlight differences in mechanism. However, the fundamental basis of allostery in each group is the same, namely antibody binding leads to a mechanical constraint in protein structure.[33]

In summary, we have shown how an antibody can inhibit enzyme activity hyperbolically by constraining conformation change. In view of the apparent correlation between antigenicity and epitope flexibility,[34] we anticipate that this mechanism will recur in allosteric effector antibodies that modulate the activities of other enzymes and receptors.

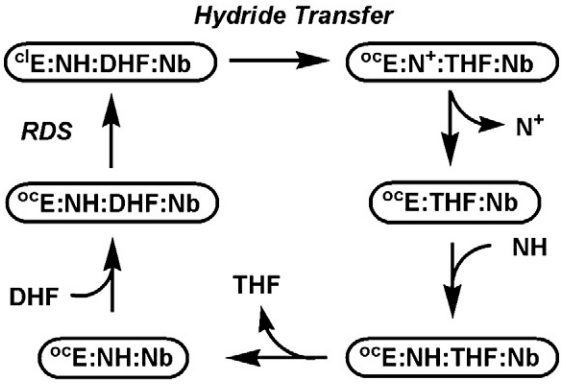

Fig. 10. Proposed catalytic intermediates of *E. coli* DHFR during steady-state turnover under saturating concentrations of substrate, cofactor, and Nb216.

Materials and Methods

General procedures

A pET22b-derived expression vector containing the coding sequence of DHFR from *E. coli* was kindly provided by Professor S. Benkovic (University of Pennsylvania). DHFR was purified according to the method described by Boehr *et al.*[17] DHF was prepared from folic acid[35] and stored at −80 °C in 5 mM HCl and 50 mM β-mercaptoethanol. Concentrations of enzymes, nanobodies, and other reagents were estimated using their molar extinction coefficients.[14]

Production of Nb216

Nb216 was isolated from a llama cDNA library by phage display. Details of the llama immunisation and cDNA library production will be published elsewhere. We used solid-phase coated DHFR for the phage display and three rounds of consecutive *in vitro* selection.

Production and purification of nanobodies

Recombinant Nb216 was produced with a C-terminal His-tag in *E. coli* WK6 and purified using Ni-affinity chromatography using standard protocols.[36] These preparations were not suitable for steady-state kinetic analysis because they contained a small amount (generally 1:10,000) of contaminating DHFR. We therefore used a DHFR knockout expression host (*E. coli* LH8, kindly provided by Professor Liz Howell, University of Tennessee). The protocol for nanobody production in the LH8 strain was identical with that used for the WK6 strain, except that LH8 cultures were grown in TB broth supplemented with kanamycin, ampicillin, and thymidine (50 μg ml^{-1}). Nb216 was stored either at 4 °C or at −20 °C in 50 mM phosphate and 150 mM NaCl (pH 7.0).

Kinetics and affinity of measurements of nanobody–DHFR interactions

Association and dissociation rate constants were measured by surface plasmon resonance (Biacore T100 and 3000) at 25 °C using nanobodies immobilised to a nickel–nitrilotriacetic acid biochip.[7]

Steady-state assays of DHFR

All assays were performed in MTEN buffer (50 mM 2-(*N*- morpholino)ethanesulfonic acid, 25 mM tris(hydroxymethyl)- aminomethane, 25 mM ethanolamine, and 100 mM NaCl, pH 7.0) at 25 °C.[14] DHFR was preincubated with NADPH for 10 min prior to addition of DHF to avoid nonlinear initial velocities. Initial rates of NADPH oxidation were corrected for background decomposition of NADPH. Assays were performed with sufficient DHFR (typically 0.5–10 nM, depending on the extent of inhibition by nanobody) to ensure that the measured velocity was >10-fold higher than the background. DHFR contamination of nanobody preparations was checked by performing the assay in the absence of added DHFR. Plots of apparent (K_m/k_{cat}) and apparent ($1/k_{cat}$) *versus* nanobody concentration were fitted to Eq. (1).[7]

Stopped flow

Stopped flow was performed either at 5 °C or at 25 °C in MTEN buffer (adjusted to pH 7.0 at 25 °C, and to pH 7.2 at 5 °C) using an Applied Photophysics SX10 stopped-flow instrument (for general details of the protocol, see Vandemeulebroucke *et al.*[37]). A dead time of 4 ms was measured at 5 °C and 25 °C. Fluorescence detection was made with either 305-nm or 400-nm cutoff filters. The molar extinction coefficient for the DHFR reaction was determined by measuring the total absorbance change upon reaction completion. In general, 10–14 progress curves were averaged. Progress curves were fitted to Eq. (3) using the program Origin:

$$y = C + Dt + \sum_{i=1}^{n} A_i \exp(-k_i t) \quad (3)$$

where $n = 1$ or 2 for monophasic and biphasic transients, respectively. Hyperbolic plots were fitted to Eq. (4):

$$k_{obs} = \frac{k_{sat}[L]}{K + [L]} \quad (4)$$

Crystallography

The E:Nb216 complex was purified by size-exclusion chromatography [Superdex-75 in 20 mM Hepes and 150 mM NaCl (pH 7.0)] and concentrated (final concentration, 0.3 mM). The DHFR:Nb216 complex was crystallised by sitting-drop vapor diffusion (298 K) in 40% vol/vol polyethylene glycol 300, 5% wt/vol polyethylene glycol 1000, and 100 mM Tris–HCl (pH 8.5; 200-nl drop). Crystals were apparent between 1 week and 2 weeks and cryopreserved directly. Data sets were collected at the Soleil-Proxima beamline. Data collection and processing statistics and methods are detailed in Table 4. Briefly, the data were processed using the HKL and CCP4 suite of programs. The structure was solved with the molecular replacement method using PHASER and further refined using REFMAC5. Interface accessible solvent areas were calculated using the ProtorP server.[22]

Table 4. Crystallography data collection and refinement parameters for DHFR:Nb216

Data collection	
Beamline	Soleil-Proxima-1
Wavelength (Å)	0.9800
Space group	$P2_12_12_1$
a	55.300
b	62.322
c	102.848
α	90.0
β	90.0
γ	90.0
Resolution range (Å)	30.0–1.90 (1.93–1.90)
Completeness (%)	99.9 (100.0)
R_{sym} (%)[a]	9.1(29.3)
Refinement statistics	
Number of protein atoms	2149
Number of water molecules	177
R-factor (%)[b]	19.5
R_{free} (%)	23.9
RMS deviation from ideality[b]	
Bonds (Å)	0.018
Angles (°)	1.746

[a] $R_{sym} = \sum(I - \langle I \rangle)/\sum(I)$, where I is the intensity measurement for a given reflection, and $\langle I \rangle$ is the average intensity for multiple measurements of this reflection.
[b] With respect to Engh and Huber parameters.

Accession number

Atomic coordinates and structure factors have been deposited in the PDB† under PDB code 3K74.

Supplementary materials related to this article can be found online at doi:10.1016/j.jmb.2011.01.017

Acknowledgements

We thank Dr. Els Pardon, Nele Buys, and Katleen Willibal for expert advice and assistance with the phage display. We are also very grateful to Professors Steve Benkovic (University of Pennsylvania) and Peter Wright (Scripps Research Institute) for their comments on an earlier version of this manuscript. This work was funded by Research Foundation—Flanders and the Flanders Interuniversity Institute for Biotechnology.

References

1. Fenton, A. W. (2008). Allostery: an illustrated definition for the 'second secret of life'. *Trends Biochem. Sci.* **33**, 420–425.
2. Cui, Q. & Karplus, M. (2008). Allostery and cooperativity revisited. *Protein Sci.* **17**, 1295–1307.
3. Goodey, N. M. & Benkovic, S. J. (2008). Allosteric regulation and catalysis emerge via a common route. *Nat. Chem. Biol.* **4**, 474–482.
4. Hardy, J. A. & Wells, J. A. (2004). Searching for new allosteric sites in enzymes. *Curr. Opin. Struct. Biol.* **14**, 706–715.
5. Shapira, E. & Arnon, R. (1967). The mechanism of inhibition of papain by its specific antibodies. *Biochemistry*, **6**, 3951–3956.
6. Pollock, M. R. (1964). Stimulating and inhibiting antibodies for bacterial penicillinase. *Immunology*, **7**, 707–723.
7. Barlow, J. N., Conrath, K. & Steyaert, J. (2009). Substrate-dependent modulation of enzyme activity by allosteric effector antibodies. *Biochim. Biophys. Acta*, **1794**, 1259–1268.
8. Celada, F. & Strom, R. (1972). Antibody-induced conformational changes in proteins. *Q. Rev. Biophys.* **5**, 395–425.
9. Dallas, M., Deuchars, S. A. & Deuchars, J. (2005). Immunopharmacology—antibodies for specific modulation of proteins involved in neuronal function. *J. Neurosci. Methods*, **146**, 133–148.
10. Casadevall, A., Dadachova, E. & Pirofski, L. a. (2004). Passive antibody therapy for infectious diseases. *Nat. Rev. Microbiol.* **2**, 695–703.
11. Makita, N., Sato, J., Manaka, K., Shoji, Y., Oishi, A., Hashimoto, M. *et al.* (2007). An acquired hypocalciuric hypercalcemia autoantibody induces allosteric transition among human Ca-sensing receptor conformations. *Proc. Natl Acad. Sci. USA*, **104**, 5443–5448.
12. May, L. T., Leach, K., Sexton, P. M. & Christopoulos, A. (2007). Allosteric modulation of G protein-coupled receptors. *Annu. Rev. Pharmacol. Toxicol.* **47**, 1–51.
13. Muyldermans, S., Baral, T. N., Cortez Retamozzo, V., De Baetselier, P., De Genst, E., Kinne, J. *et al.* (2009). Camelid immunoglobins and nanobody technology. *Vet. Immunol. Immunopathol.* **128**, 178–183.
14. Fierke, C. A., Johnson, K. A. & Benkovic, S. J. (1987). Construction and evaluation of the kinetic scheme associated with dihydrofolate reductase from *Escherichia coli*. *Biochemistry*, **26**, 4085–4092.
15. Schnell, J. R., Dyson, H. J. & Wright, P. E. (2004). Structure, dynamics, and catalytic function of dihydrofolate reductase. *Annu. Rev. Biophys. Biomol. Struct.* **33**, 119–140.
16. Sawaya, M. R. & Kraut, J. (1997). Loop and subdomain movements in the mechanism of *Escherichia coli* dihydrofolate reductase: crystallographic evidence. *Biochemistry*, **36**, 586–603.
17. Boehr, D. D., McElheny, D., Dyson, H. J. & Wright, P. E. (2006). The dynamic energy landscape of dihydrofolate reductase. *Science*, **313**, 1638–1642.
18. Wolfenden, R. (1974). Enzyme catalysis: conflicting requirements of substrate access and transition state affinity. *Mol. Cell Biochem.* **3**, 207–211.
19. Hammes-Schiffer, S. & Benkovic, S. J. (2006). Relating protein motion to catalysis. *Annu. Rev. Biochem.* **75**, 519–541.
20. Monod, J., Changeux, J. P. & Jacob, F. (1963). Allosteric proteins and cellular control systems. *J. Mol. Biol.* **6**, 306–329.
21. Cornish-Bowden, A. (1995). *Fundamentals of Enzyme Kinetics*, Revised Edition. Portland Press Ltd., London, UK.
22. Reynolds, C., Damerell, D. & Jones, S. (2009). ProtorP: a protein–protein interaction analysis server. *Bioinformatics*, **25**, 413–414.
23. Cameron, C. E. & Benkovic, S. J. (1997). Evidence for a functional role of the dynamics of glycine-121 of *Escherichia coli* dihydrofolate reductase obtained from kinetic analysis of a site-directed mutant. *Biochemistry*, **36**, 15792–15800.
24. Cooper, A. & Dryden, D. T. F. (1984). Allostery without conformation change. *Eur. Biophys. J.* **11**, 103–109.
25. Freire, E. (1999). The propagation of binding interactions to remote sites in protein: analysis of the binding of the monoclonal antibody D1.3 to lysozyme. *Proc. Natl Acad. Sci. USA*, **96**, 10118–10122.
26. Williams, D. C., Benjamin, D. C., Poljak, R. J. & Rule, G. S. (1996). Global changes in amide hydrogen exchange rates for a protein antigen in complex with three different antibodies. *J. Mol. Biol.* **257**, 866–876.
27. Sundberg, E. J. & Mariuzza, R. A. (2003). Molecular recognition in antibody–antigen complexes. *Adv. Protein Chem.* **61**, 119–160.
28. Koide, S. (2009). Engineering of recombinant crystallisation chaperones. *Curr. Opin. Struct. Biol.* **19**, 449–457.
29. Murali, R., Sharkey, D. J., Daiss, J. L. & Murthy, H. M. K. (1998). Crystal structure of Taq DNA polymerase in complex with an inhibitory Fab: the Fab is directed against an intermediate in the helix–coil dynamics of the enzyme. *Proc. Natl Acad. Sci.* **95**, 12562–12567.

† www.pdb.org

30. Wien, M. W., Filman, D. J., Stura, E. A., Guillot, S., Delpeyroux, F., Crainic, R. & Hogle, J. M. (1995). Structure of the complex between the Fab fragment of a neutralizing antibody for type 1 poliovirus and its viral epitope. *Nat. Struct. Biol.* **2**, 232–242.
31. Ganesan, R., Eigenbrot, C., Wu, Y., Liang, W. C., Shia, S., Lipari, M. T. & Kirchhofer, D. (2009). Unraveling the allosteric mechanism of serine protease inhibition by an antibody. *Structure*, **17**, 1614–1624.
32. Horn, J. R. & Shoichet, B. K. (2004). Allosteric inhibition through core disruption. *J. Mol. Biol.* **336**, 1283–1291.
33. Sachs, D. H., Schechter, A. N., Eastlake, A. & Anfinsen, C. B. (1972). An immunological approach to the conformational equilibria of polypeptides. *Proc. Natl Acad. Sci. USA*, **69**, 3790–3794.
34. Paus, D. & Winter, G. (2006). Mapping epitopes and antigenicity by site-directed masking. *Proc. Natl Acad. Sci. USA*, **103**, 9172–9177.
35. Blakley, R. L. (1960). Crystalline dihydropteroylglutamic acid. *Nature*, **188**, 231–232.
36. Conrath, K., Vincke, C., Stijlemans, B., Schymkowitz, J., Decanniere, K., Wyns, L. *et al.* (2005). Antigen binding and solubility effects upon the veneering of a camel VHH in framework-2 to mimic a VH. *J. Mol. Biol.* **350**, 112–125.
37. Vandemeulebroucke, A., Versées, W., Steyaert, J. & Barlow, J. N. (2006). Multiple transients in the pre-steady state of nucleoside hydrolase reveal complex substrate binding, product base release and two apparent rates of chemistry. *Biochemistry*, **45**, 9307–9318.